Quench-Induced Supercurrents in an Annular Bose Gas

L. Corman,[1] L. Chomaz,[1,4] T. Bienaimé,[1] R. Desbuquois,[2] C. Weitenberg,[3]
S. Nascimbène,[1] J. Dalibard,[1,4] and J. Beugnon[1,*]
[1]Laboratoire Kastler Brossel, CNRS, UPMC, ENS, Collège de France, 24 Rue Lhomond, 75231 Paris Cedex 05, France
[2]Institut für Quantenelektronics, ETH Zurich, 8093 Zurich, Switzerland
[3]Institut für Laserphysik, Universität Hamburg, Luruper Chaussee 149, D-22761 Hamburg, Germany
[4]Collège de France, 11 Place Marcelin Berthelot, 75005 Paris, France
(Received 16 June 2014; published 26 September 2014)

We create supercurrents in annular two-dimensional Bose gases through a temperature quench of the normal-to-superfluid phase transition. We detect the magnitude and the direction of these supercurrents by measuring spiral patterns resulting from the interference of the cloud with a central reference disk. These measurements demonstrate the stochastic nature of the supercurrents. We further measure their distribution for different quench times and compare it with predictions based on the Kibble-Zurek mechanism.

DOI: 10.1103/PhysRevLett.113.135302 PACS numbers: 67.85.-d, 03.75.Kk, 03.75.Lm, 64.60.an

Fluids in annular geometry are ideally suited to investigate the role of topological numbers in quantum mechanics. The phase winding of the macroscopic wave function around the annulus must be a multiple of 2π, ensuring the quantization of the circulation of the fluid velocity. The resulting supercurrents have been observed in superfluid systems such as superconductors [1], liquid helium [2], and atomic gases [3,4]. Studying these currents is crucial for the understanding of quantum fluids as well as for realizing sensitive detectors like magnetometers [5] and rotation sensors [6].

Supercurrents in annular atomic Bose-Einstein condensates (BECs) are usually created in a deterministic way by using laser beams to impart angular momentum on the atoms [3,4,7] or by rotating a weak link along the annulus [8]. Supercurrents can also have a stochastic origin. They may result from thermal fluctuations or appear as topological defects following a rapid quench of the system. The latter mechanism was put forward by Kibble and Zurek (KZ), who studied the phase patterns that emerge in a fluid, when it undergoes a fast crossing of a phase transition point [9,10].

The KZ mechanism has been studied in several types of systems such as liquid crystals [11], helium [12,13], ion chains [14,15], superconducting loops [16], and BECs [17–19]. For a superfluid confined in a ring geometry, which is the configuration originally considered by Zurek [9], the frozen phase of the wave function may lead to a supercurrent of charge q, i.e., a $2\pi q$ phase winding along the ring. In this Letter, we study a setup realizing this gedanken experiment using a quasi-two-dimensional (2D) Bose gas trapped in an annular geometry. For each realization of the experiment, we use matter-wave interference between this annulus and a central disk acting as a phase reference, to measure the charge as well as the direction of the random supercurrent [20].

Our experiments are performed with a Bose gas of ^{87}Rb atoms. Along the vertical (z) direction, the gas is confined using a harmonic potential with frequency $\omega_z/2\pi = 370$ Hz [Fig. 1(a)] (Supplemental Material [21]). In the horizontal (xy) plane, the atoms are trapped in the dark regions of a "box-potential" beam, engineered using an intensity mask located in a plane optically conjugated to the atom cloud [27]. We use a targetlike mask, consisting of a disk of radius $R_0 = 4.5$ μm surrounded by a ring of inner (respective outer) radius of $R_{\rm in} = 9$ μm (respective $R_{\rm out} = 15$ μm) [Fig. 1(b)].

The typical time sequence for preparing the gas starts by loading a gas with a three-dimensional (3D) phase-space density ≈ 2.4 slightly below the condensation threshold [29] with the box-potential beam at its maximal power. Then we linearly lower this power by a factor ~ 50 in a time $t_{\rm evap}$ to evaporatively cool the atomic cloud and cross the superfluid transition [30]. Last, we keep the atoms at a constant box-potential depth during a time $t_{\rm hold}$. The final temperature is ~ 10 nK with similar surface densities in the ring and the disk: $\rho \sim 80$ μm^{-2}. The typical interaction energy per atom is $E_{\rm int}/k_{\rm B} \approx 8$ nK, and the gas is marginally quasi-2D with $k_{\rm B}T$, $E_{\rm int} \sim \hbar\omega_z$. These parameters correspond to a large 2D phase-space density $\mathcal{D} = \rho\lambda^2 \geq 100$ so that the gas is deeply in the superfluid regime at the end of the evaporation ramp ($\lambda = [2\pi\hbar^2/(mk_{\rm B}T)]^{1/2}$ is the thermal wavelength and m the mass of the ^{87}Rb atom).

We use matter-wave interference to probe the relative phase distribution between the cloud in the central disk and the one in the ring. We abruptly switch off the box potential while keeping the confinement along the z direction. The clouds experience a hydrodynamical expansion during which the initial interaction energy is converted into kinetic energy. After 7 ms of expansion, we record the interference pattern by imaging the atomic gas along the vertical

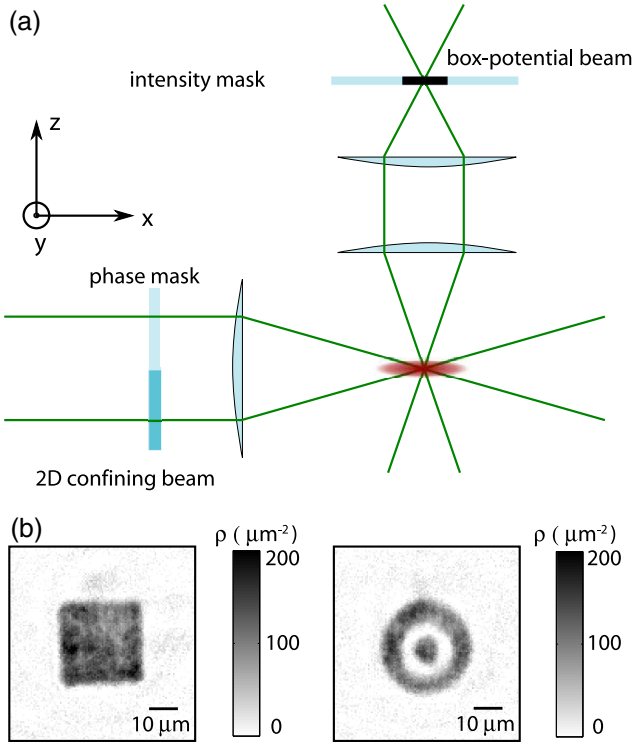

FIG. 1 (color online). Production of boxlike potentials using an intensity mask. (a) Along the vertical direction, atoms are confined by a laser beam with an intensity node in the plane $z = 0$, which is shaped using a phase plate (π phase shift between the upper and lower halves of the phase plate). In plane, atoms are trapped in boxlike potentials created by imaging an intensity mask onto the atomic plane. (b) *In situ* images of uniform gases in the square and target potentials.

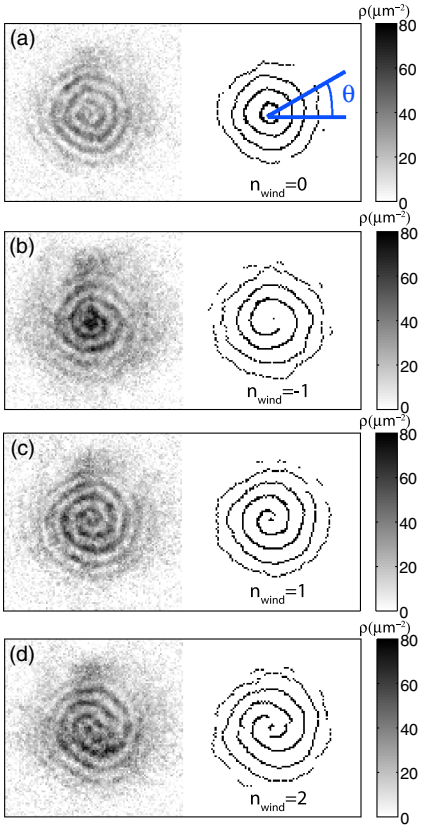

FIG. 2 (color online). Experimental interference patterns. Examples of interference patterns after expansion in the 2D plane, along with contrast-amplified pictures; (a) without phase winding, (b) with phase winding -2π, (c) with phase winding $+2\pi$, (d) with phase winding $+4\pi$.

direction. Typical interference patterns are shown in Fig. 2. Most of them consist in concentric rings, as expected for a quasiuniform phase distribution in the disk and the annulus. However we also observe a significant fraction of spiral patterns, revealing the presence of a phase winding in the wave function of one of the two clouds.

We developed an automatized procedure to analyze these patterns, which reconstructs the phase $\phi(\theta)$ of the fringes along a line of azimuthal angle θ (see the Supplemental Material [21]). From the accumulated phase $\Delta\phi$ as the angle θ varies from 0 to 2π, we associate to each pattern a winding number $n_{\mathrm{wind}} = \Delta\phi/2\pi$, which is a positive, null, or negative integer. This number is recorded for many realizations of the same experimental sequence. Examples of the probability distribution of n_{wind} are shown in Figs. 3(a) and 3(b). The measured histograms are compatible with a zero mean value [31]. For example, if we use all the data presented in Figs. 3(c) and 3(d) we find $\langle n_{\mathrm{wind}} \rangle = 0.002(20)$. This confirms the stochastic nature of the mechanism at the origin of this phase winding.

The first question that arises is the origin of the observed phase winding, which can be due either to a vortex in the central disk or to a quantized persistent current in the outer ring. We can experimentally eliminate the first possibility by noticing that when doing a 3D ballistic expansion (by switching off both the box-potential beam and the confining beam in the z direction) we never observe any vortex signature in the small disk of radius $R_0 = 4.5\ \mu$m. By contrast, in larger structures such as the square represented in Fig. 1(b), we can detect deep density holes revealing the presence of vortices [32]. Hence, we conclude that the spiral interference patterns of Fig. 2 reveal the presence of a supercurrent in the annulus, whose charge and orientation correspond to the modulus and sign of the winding number n_{wind}. The lifetime of this supercurrent is similar to the cloud lifetime [see Fig. 3(c)].

We now discuss the origin of the observed supercurrents, which can be either thermal excitations or result from the quench cooling. If these currents had a thermal origin, their probability of occurrence would be given by the Boltzmann law $p(n_{\mathrm{wind}}) \propto \exp[-E(n_{\mathrm{wind}})/k_B T]$, where the (kinetic) energy of the supercurrent is

$$E(n_{\mathrm{wind}}) = n_{\mathrm{wind}}^2 \frac{\pi\hbar^2\rho}{m} \ln(R_{\mathrm{out}}/R_{\mathrm{in}}). \quad (1)$$

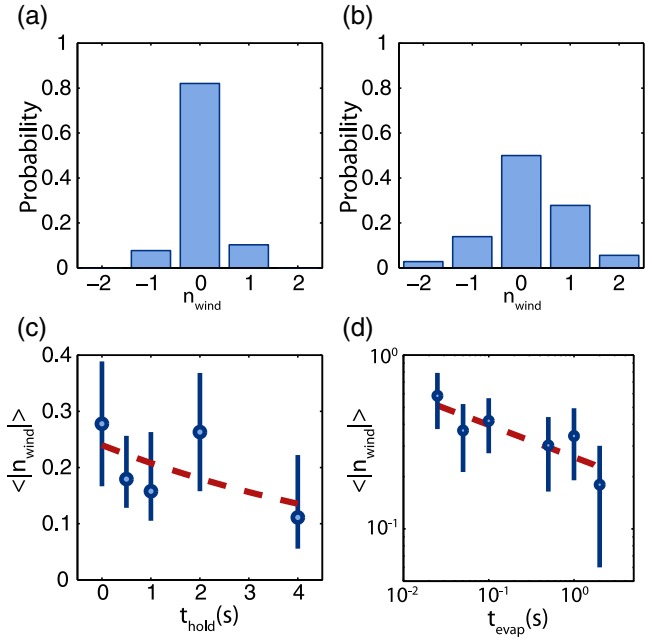

FIG. 3 (color online). Study of the winding number. [(a) and (b)] Histograms showing the statistical appearance of winding number n_{wind} for $t_{\mathrm{hold}} = 0.5$ s. (a) We show the result of 39 realizations for $t_{\mathrm{evap}} = 2$ s. We get $\langle n_{\mathrm{wind}} \rangle = 0.03(8)$. (b) We show the result of 36 realizations for $t_{\mathrm{evap}} = 0.025$ s. We get $\langle n_{\mathrm{wind}} \rangle = 0.19(14)$. (c) Mean absolute winding number $\langle |n_{\mathrm{wind}}| \rangle$ as a function of hold time ($t_{\mathrm{evap}} = 2$ s). The data are fitted with an exponential with a time constant of 7 s. (d) Mean absolute winding number $\langle |n_{\mathrm{wind}}| \rangle$ as a function of evaporation time ($t_{\mathrm{hold}} = 0.5$ s) in log-log scale. The line is a power-law fit to the data; $\langle |n_{\mathrm{wind}}| \rangle \propto t_{\mathrm{evap}}^{-\alpha}$, which gives $\alpha = 0.19(6)$. The uncertainty on $\langle n_{\mathrm{wind}} \rangle$ and the bars on (c) and (d) represent the statistical error determined with a bootstrapping approach described in the Supplemental Material [21].

This leads to

$$p(n_{\mathrm{wind}}) \propto (R_{\mathrm{in}}/R_{\mathrm{out}})^{n_{\mathrm{wind}}^2 \mathcal{D}/2}, \tag{2}$$

which is negligible for $n_{\mathrm{wind}} \neq 0$ for our large phase space densities $\mathcal{D} \geq 100$, in clear disagreement with the typical 20%–50% of pictures showing phase winding. Note that the probability for a vortex to appear in the central disk as a thermal excitation is even smaller than that of Eq. (2) because R_{in} and R_{out} should be replaced respectively by the healing length ($\lesssim 0.5$ μm) and R_0.

To check that the quench cooling is indeed responsible for the formation of these supercurrents, we study the variation of $\langle |n_{\mathrm{wind}}| \rangle$ for evaporation times spanning two orders of magnitude. The comparison between the results for a slow quench [Fig. 3(a)] and a fast quench [Fig. 3(b)] show that the latter, indeed, increases the probability of occurrence of a supercurrent, as expected for the KZ mechanism [9,10]. We summarize in Fig. 3(d) the experimental variation of $\langle |n_{\mathrm{wind}}| \rangle$ with t_{evap} and find that it increases from 0.2 ($t_{\mathrm{evap}} = 2$ s) to 0.6 ($t_{\mathrm{evap}} = 0.025$ s). A power-law fit to the data, inspired by the prediction for the KZ mechanism, leads to $\langle |n_{\mathrm{wind}}| \rangle \propto t_{\mathrm{evap}}^{-\alpha}$ with $\alpha = 0.19(6)$.

To interpret our results, we have developed a simple one-dimensional (1D) model following the KZ scenario presented in Refs. [9,33]. We consider a 1D ring of perimeter L, and we assume that, when the normal-to-superfluid transition is crossed, N domains of uniform phase ϕ_j, $j = 1, \ldots, N$ are created. Each run of the experiment is modeled by a set $\{\phi_j\}$, where the phases ϕ_j are independent random variables drawn in $(-\pi, \pi]$ (with $\phi_1 = 0$ by convention). For each set of $\{\phi_j\}$, we calculate the total phase variation along the ring $\Phi = \sum_j \phi_j$ and define n_{wind} as the nearest integer to $\Phi/2\pi$. We then average over many draws of the set $\{\phi_j\}$. Our experimental range $0.2 \leq \langle |n_{\mathrm{wind}}| \rangle \leq 0.6$ is obtained for $3 \leq N \leq 10$, corresponding to the approximate power-law scaling (see the Supplemental Material [21])

$$\langle |n_{\mathrm{wind}}| \rangle \propto N^{0.8}. \tag{3}$$

Then we use the general prediction for the KZ mechanism to relate the typical length $\hat{\xi} = L/N$ of a domain to the quench time t_{evap} (see e.g., Ref. [33])

$$\hat{\xi} \propto t_{\mathrm{evap}}^{\nu/(1+\nu z)}, \tag{4}$$

where ν and z define the universality class of the transition: ν is the correlation length critical exponent and z is the dynamic critical exponent. Using $z = 2$ and $\nu = 1/2$ relevant for a mean-field description of a 1D ring-shaped system [33], we get

$$\hat{\xi} = \frac{L}{N} \propto t_{\mathrm{evap}}^{1/4}. \tag{5}$$

Combining Eqs. (3) and (5), we predict with this simple model

$$\langle |n_{\mathrm{wind}}| \rangle \propto t_{\mathrm{evap}}^{-1/4 \times 0.8} \approx t_{\mathrm{evap}}^{-0.2}, \tag{6}$$

which is in agreement with the experimental result of $\alpha = 0.19(6)$.

There are two main assumptions that could limit the validity of this model. First, our system is not unidimensional in terms of relevant single particle eigenstates. However, we find for our parameters that $\hat{\xi}$ is in the range of 7–25 μm [34,35]; this is always larger than the width of our annulus and justifies the use of a 1D model for describing the phase coherence properties of the gas. Second, this model does not take into account beyond mean-field effects, related to either the finite size of the system or the crossover between standard BEC and the Berezinskii-Kosterlitz-Thouless mechanism. This could change the value of the critical exponents and even lead to deviations with respect to the power-law scaling of Eq. (4) [36].

We now discuss the possible extension of this work to a more thorough test of the KZ mechanism. Power-law scaling is challenging to test in our situation because of the low value of the exponent (≈ 0.2) even if we span 2 orders of magnitude for t_{evap}. The extreme values of this range are experimentally limited. (i) The evaporation time t_{evap} should be chosen long enough so that at any given time a local thermal equilibrium is achieved in the cloud (see the Supplemental Material [21]). (ii) The largest evaporation time is set by the cloud lifetime. These two limits cannot be significantly modified, which fixes the relative range of variation of the number of domains N. It could also be interesting to study situations with absolute larger $N = L/\hat{\xi}$. For a given density, the local equilibrium requirement limits the lower value of $\hat{\xi}$, and one can only increase the length of the ring L. Within current experimental techniques, it should be possible to load one order of magnitude more atoms, leading for a given transverse size to an increase of N by the same factor.

In the last part of this Letter, we show that one can extract information from the interference patterns, which goes beyond the determination of the topological number n_{wind}. In particular, the ripples of the fringes are related to the phase distribution of the fluids in the central disk and the ring, which is characterized by the one-body correlation function g_1. This function plays a specially important role for low-dimensional systems, since it indicates how long-range order is destroyed by thermal phonons. To give an estimate of g_1, we study the angular dependance of the phase of the fringes $\phi(\theta)$ as shown in Fig. 4(a). In particular we consider the periodic function $\delta\phi(\theta) = \phi(\theta) - n_{\mathrm{wind}}\theta$, which describes the deviation of the reconstructed phase from a perfect linear winding. We construct the angular correlation function

$$g_1^{(\mathrm{exp})}(\theta) = \langle e^{i[\delta\phi(\theta')-\delta\phi(\theta'+\theta)]}\rangle_{\theta',\ \mathrm{realizations}}, \qquad (7)$$

where the average is taken over all images irrespective of the value of n_{wind}, and which is expected to be real in the limit of a large number of realizations. A typical example for $\mathrm{Re}[g_1^{(\mathrm{exp})}]$ is given in Fig. 4(b), where the minimum for $\theta = \pi$ gives an indication of the phase coherence between diametrically opposite points. This measured angular correlation function $g_1^{(\mathrm{exp})}(\theta)$ can be used to reconstruct the first-order correlation function of the gas in the annulus (see Supplemental Material [21]). This correlation function could allow one to extract the evolution of the phonon distribution during the thermalization of the fluid.

In summary, we have created supercurrents in annular Bose gases by a temperature quench. The measured distribution of direction and magnitude of these supercurrents are compatible with the KZ mechanism's predictions. This work could be extended to more refined tests of the KZ mechanism by testing the power-law scaling with the size of the annulus and correlating the number of topological defects with the condensed fraction of the system [33].

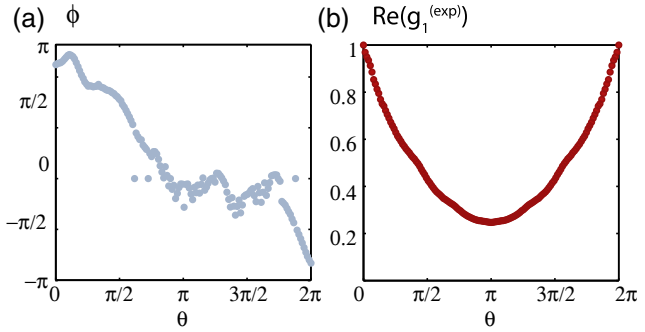

FIG. 4 (color online). Analysis of the phase profiles. (a) Typical phase distribution reconstructed from the phase profile $\phi(\theta)$ of the interference pattern of Fig. 2(b) showing a winding number of -1. (b) Real value of the angular correlation function reconstructed from the phase of the interference patterns with 18 realizations of $t_{\mathrm{evap}} = 2$ s and $t_{\mathrm{hold}} = 4$ s. When $n_{\mathrm{wind}} \neq 0$, the linear phase winding is subtracted before computing g_1.

We thank J. Palomo and D. Perconte for the realization of the intensity masks and Z. Hadzibabic for useful discussions. This work is supported by IFRAF, ANR (ANR-12-BLANAGAFON), and ERC (Synergy UQUAM) and the Excellence Cluster CUI. L. Ch. and L. Co. acknowledge the support from DGA, and C. W. acknowledges the support from the EU (PIEF-GA-2011- 299731). L. Co. and L. Ch. contributed equally to this work.

*beugnon@lkb.ens.fr

[1] A. H. Silver and J. E. Zimmerman, Phys. Rev. **157**, 317 (1967).
[2] P. J. Bendt, Phys. Rev. **127**, 1441 (1962).
[3] C. Ryu, M. F. Andersen, P. Cladé, V. Natarajan, K. Helmerson, and W. D. Phillips, Phys. Rev. Lett. **99**, 260401 (2007).
[4] S. Moulder, S. Beattie, R. P. Smith, N. Tammuz, and Z. Hadzibabic, Phys. Rev. A **86**, 013629 (2012).
[5] J. Clarke, *Superconductor Applications: SQUIDs and Machines*, edited by B. B. Schwartz and S. Foner (Plenum, New York, 1977).
[6] R. E. Packard and S. Vitale, Phys. Rev. B **46**, 3540 (1992).
[7] S. Beattie, S. Moulder, R. J. Fletcher, and Z. Hadzibabic, Phys. Rev. Lett. **110**, 025301 (2013).
[8] K. C. Wright, R. B. Blakestad, C. J. Lobb, W. D. Phillips, and G. K. Campbell, Phys. Rev. Lett. **110**, 025302 (2013).
[9] W. H. Zurek, Nature (London) **317**, 505 (1985).
[10] T. W. B. Kibble, J. Phys. A **9**, 1387 (1976).
[11] I. Chuang, B. Yurke, R. Durrer, and N. Turok, Science **251**, 1336 (1991).
[12] V. M. H. Ruutu, V. B. Eltsov, A. J. Gill, and T. W. B. Kibble, Nature (London) **382**, 334 (1996).
[13] C. Bäuerle, Y. M. Bunkov, and S. N. Fisher, Nature (London) **382**, 332 (1996).
[14] S. Ulm, J. Roßnagel, G. Jacob, C. Degünther, S. T. Dawkins, U. G. Poschinger, R. Nigmatullin, A. Retzker, M. B. Plenio,

F. Schmidt-Kaler, and K. Singer, Nat. Commun. **4**, 2290 (2013).
[15] K. Pyka, J. Keller, H. Partner, R. Nigmatullin, T. Burgermeister, D. M. Meier, K. Kuhlmann, A. Retzker, M. Plenio, W. Zurek, A. del Campo, and T. Mehlstäubler, Nat. Commun. **4**, 2291 (2013).
[16] R. Monaco, J. Mygind, R. J. Rivers, and V. P. Koshelets, Phys. Rev. B **80**, 180501 (2009).
[17] C. Weiler, T. Neely, D. Scherer, A. Bradley, M. Davis, and B. Anderson, Nature (London) **455**, 948 (2008).
[18] G. Lamporesi, S. Donadello, S. Serafini, F. Dalfovo, and G. Ferrari, Nat. Phys. **9**, 656 (2013).
[19] S. Braun, M. Friesdorf, S. S. Hodgman, M. Schreiber, J. P. Ronzheimer, A. Riera, M. del Rey, I. Bloch, J. Eisert, and U. Schneider, arXiv:1403.7199.
[20] A similar method has recently been developed to investigate the supercurrent generated by a rotating weak link [37].
[21] For details, see the Supplemental Material at http://link.aps.org/supplemental/10.1103/PhysRevLett.113.135302, which includes Refs [22–26].
[22] Y.-J. Lin, A. R. Perry, R. L. Compton, I. B. Spielman, and J. V. Porto, Phys. Rev. A **79**, 063631 (2009).
[23] G. Reinaudi, T. Lahaye, Z. Wang, and D. Guéry-Odelin, Opt. Lett. **32**, 3143 (2007).
[24] L. Chomaz, L. Corman, T. Yefsah, R. Desbuquois, and J. Dalibard, New J. Phys. **14**, 055001 (2012).
[25] B. Efron, J. Am. Stat. Assoc. **82**, 171 (1987).
[26] W. Ketterle and N. van Druten, Adv. At. Mol. Opt. Phys. **37**, 181 (1996).
[27] See Ref. [28] for a 3D version of a similar setup.
[28] A. Gaunt, T. F. Schmidutz, I. Gotlibovych, R. P. Smith, and Z. Hadzibabic, Phys. Rev. Lett. **110**, 200406 (2013).
[29] The estimated total atom number is 76 000, and the temperature is 210 nK. With these parameters, we never observe any interference fringes such as those of Fig. 2.
[30] R. Desbuquois, L. Chomaz, T. Yefsah, J. Léonard, J. Beugnon, C. Weitenberg, and J. Dalibard, Nat. Phys. **8**, 645 (2012).
[31] The observed asymmetry on Fig. 3(b) (mean value is 1.4 times the standard deviation) is compatible with the number of realizations: the probability to have a standard deviation equal or larger than this one is 17%.
[32] L. Chomaz *et al.* (to be published).
[33] A. Das, J. Sabbatini, and W. Zurek, Sci. Rep. **2**, 352 (2012).
[34] An estimate of $\hat{\xi}$ for our geometry is $\pi(R_{\rm in}+R_{\rm out})/N$.
[35] We note that $\hat{\xi}$ is then larger than the size R_0 of the central disk. This confirms the fact that we do not expect the presence of vortices in this disk.
[36] A. Jelic and L. Cugliandolo, J. Stat. Mech. (2011) P02032.
[37] S. Eckel, F. Jendrzejewski, A. Kumar, C. Lobb, and G. Campbell, arXiv:1406.1095 [Phys. Rev. X (to be published)].